Optical Materials 88 (2019) 635–641

Contents lists available at ScienceDirect

Optical Materials

journal homepage: www.elsevier.com/locate/optmat

Widening the emission spectrum of Eu^{2+} in $Na_3Sc_2(PO_4)_3$ to full-color via controlling the multi-emission centers by equivalent substitution of Sc−Al and PO_4-BO_3

Dong Liu, Yahong Jin*, Haoyi Wu, Guifang Ju, Yang Lv, Li Chen, Yihua Hu**

School of Physics and Optoelectronic Engineering, Guangdong University of Technology, WaiHuan Xi Road, No. 100, Guangzhou, 510006, China

ARTICLE INFO

Keywords:
Equivalent substitution
Color tunable
Phosphor
Polyhedron distortion

ABSTRACT

Single-doped color tunable phosphors $Na_3Sc_{2-x}Al_x(PO_4)_{3-y}(BO_3)_y:Eu^{2+}$ are synthesized by conventional high temperature solid-state reaction method. Both the excitation and emission spectra of Eu^{2+} in $Na_3Sc_2(PO_4)_3$ can be effectively tailored by equivalent substitution. The equivalent cation substitution of Sc^{3+} by Al^{3+} and unit substitution of $(PO_4)^{3-}$ by $(BO_3)^{3-}$ results in the significant distortion of the local environment neighboring the Na−O polyhedral, which enables the modulation of Eu^{2+} occupation on three kinds of Na sites. Besides the original occupation of Na1 site by Eu^{2+}, equivalent cation and unit substitutions open a way for Na2 and Na3 sites to be occupied by Eu^{2+} ions, which leads to the significant widening of the Eu^{2+} emission spectrum to full-color. The mechanism of widening the Eu^{2+} emission spectrum is elucidated. Furthermore, the different thermal stability behaviors that Eu1 emission is better than that of Eu2 and Eu3 ions are also discussed.

1. Introduction

Due to the superior and outstanding features, such as long life time, energy saving, environmental friendliness, high efficiency and reliability, the white light-emitting diodes (w-LEDs) are considered to a new revolution in the field of lighting source [1–4]. At present, the major commercial w-LEDs are based on blue InGaN chip and a yellow phosphor ($Y_3Al_5O_{12}:Ce^{3+}$). Unfortunately, this type of w-LED is not suitable for indoor lighting use, because the low color rendering index and high correlated color temperature [5]. As an alternative way, the combination the multiple color emitting phosphors with a near-UV (350–420 nm) LED chip may create white light with high quality for indoor illumination. However, this method of white light generation by mixing of different phosphors has some inherent drawbacks: the complex ratio control of phosphors, different excitation ranges and lower luminescence efficiency owing to the usually inevitable strong energy re-absorption. In order to avoid these problems, single-phase full-color emitting phosphors, such as $A_3MgSi_2O_8:Eu^{2+}$, Mn^{2+} (A = Ca, Sr, Ba), $Sr_3B_2O_6:Ce^{3+}$, Eu^{2+}, $NaSr_4(BO_3)_3:Ce^{3+}$, Mn^{2+}, $Ca_3Gd_7(PO_4)(SiO_4)_5O_2:Ce^{3+}$, Tb^{3+}, Mn^{2+}, $BaMg_2Al_6Si_9O_{30}:Eu^{2+}$, Tb^{3+}, Mn^{2+} and so on [6–9] have attracted much attentions. The single-phase white-emitting phosphors are usually achieved by doping multi rare-earth/transition metal ions. But, the energy transfer between sensitizer and activator will lead to energy loss, while the distinct temperature-dependent behaviors of emission centers will bring about color deviation at high temperature (150–200 °C) during the working of LED package [10]. Hence, it is necessary to develop the single-doped single-phase full-color emitting phosphors.

As one of the most widely used activators, Eu^{2+} ions show typical f–d transitions [11]. The luminescence wavelength of Eu^{2+} varies from UV to blue, yellow and even red depending on the crystal filed environment [12]. Based on these excellent luminescence properties of Eu^{2+}, the single phase white-emitting phosphor by single doping Eu^{2+} can be achieved by adjusting crystal field. There are two main methods to realize tunable emission color: one method is adjusting the concentration of Eu^{2+} ($KCaGd(PO_4)_2:Eu^{2+}$ [13], $Sr_5(PO_4)_2SiO_4:Eu^{2+}/Ce^{3+}$ [14]), another is adjusting the crystal filed by replacing the cation or anion ($Li(Sr,Ca)_4(BO_3)_3:Eu^{2+}$) [15]. Compared the two methods, realizing the color tunable luminescence by modulating the host components is more effective. In recent, a blue phosphor Eu^{2+}-doped $Na_3Sc_2(PO_4)_3$ (NSPO) with many excellent properties was reported [16–18], which arouses considerable research interest. However, all these studies concentrate on the blue emission of Eu^{2+} in one kind of Na sites. In fact, NSPO crystallizes is monoclinic system structure possess three different Na sites (Na1, Na2 and Na3), which gives us the opportunity to obtain color-tunable emission and widen the emission

* Corresponding author.
** Corresponding author.
E-mail addresses: yhjin@gdut.edu.cn (Y. Jin), huyh@gdut.edu.cn (Y. Hu).

https://doi.org/10.1016/j.optmat.2018.12.038
Received 12 November 2018; Received in revised form 10 December 2018; Accepted 22 December 2018
0925-3467/ © 2018 Elsevier B.V. All rights reserved.

spectrum by suitable changing of the Eu^{2+} occupation.

In this work, we report a single-doped single-phase $Na_3Sc_{2-x}Al_x(PO_4)_{3-y}(BO_3)_y$:0.03$Eu^{2+}$ phosphor has been prepared by high-temperature solid-state reaction method. The phase purity of the phosphor is investigated by powder X-ray diffraction (XRD) measurement. The substitution of Al^{3+} and $(BO_3)^{3-}$ for Sc^{3+} and $(PO_4)^{3-}$, respectively, cause a huge change of the local environment around Na ions, which enables the significant widening of Eu^{2+} emission spectrum. The tailoring of Eu^{2+} emission spectrum is affirmed to the occupation of Na2 and Na3 sites by Eu^{2+} ions, which is due to the expansion of Na2—O and Na3—O bonds creating larger space for Eu^{2+}. Meanwhile, the different temperature dependence behaviors of three different emission centers are discussed. A case study of $Na_3Sc_{2-x}Al_x(PO_4)_{3-y}(BO_3)_y$:0.03$Eu^{2+}$ may provide a way to design full-color emitting phosphor based on the single-doped single-phase method.

2. Experimental

2.1. Materials and synthesis

The polycrystalline samples of $Na_3Sc_{2-x}Al_x(PO_4)_3$:0.03Eu^{2+} (NSA_xP) ($0 \le x \le 1$) and $Na_3Sc_2(PO_4)_{3-y}(BO_3)_y$:0.03$Eu^{2+}$ ($NSPB_y$) ($0 \le y \le 1$) were synthesized by the conventional high temperature solid-state method. The Na_3PO_4 (99.8%), Sc_2O_3 (99.99%), $NH_4H_2PO_4$ (99.0%), Eu_2O_3 (99.9%), Al_2O_3 (analytically pure), HBO_3 (analytically pure) were used as the raw materials and weighted in stoichiometric proportions. After mixing and grinding in an agate mortar for 30 min, the mixtures were pre-sintered at 300 °C for 1 h in a muffle furnace. The mixtures were reground in an agate mortar for 15 min and then sintered at 1300 °C for 5 h under a reductive atmosphere (10% H_2 + 90% N_2). After cooling to room temperature, the prepared phosphors were reground for further measurements.

2.2. Measurements and characterization

The phase purity of the samples were verified by powder X-ray diffraction (XRD Beijing, Puxi XD-2) measurement using Cu Kα irradiation (λ = 1.5406 Å) at 36 kV tube voltage and 20 mA tube current with a scanning step of 0.02° over the 2θ range from 10° to 70°. Room-temperature photoluminescence (PL), PL excitation (PLE) spectra and decay curves were measured with a high-resolution spectrofluorometer (UK, Edinburgh Instruments, FLS980) equipped with a 500 W Xenon lamp as an excitation source, with a Hamamatsu R928P visible (VIS) photomultiplier (250–850 nm) as the detectors. The luminescence properties at elevated temperatures from 303 to 523 K were obtained using the FLS-980 fluorescence spectrophotometer equipped with an external heating setup (TAP-02). The temperature-dependent decay curves were recorded by the high-resolution spectrofluorometer equipped with a nF920 lamp (UK, Edinburgh Instruments, nF920) as an excitation source.

3. Results and discussions

3.1. Crystal structure

The crystal structure of the obtained samples were characterized by the powder XRD. Fig. 1 displays the typical XRD patterns of as-prepared phosphors NSA_xP:0.03Eu^{2+} (x = 0.5, 0.8 and 1) and $NSPB_y$:0.03Eu^{2+} (y = 0.3, 0.5 and 1) together with the standard data of NSPO (JCPDS#44–0567) as a reference. It clearly indicates that all the diffraction peaks of the obtained samples can be well indexed to the standard data of JCPDS 44–0567 without obvious change by the incorporation of Al^{3+} or $(BO_3)^{3-}$. Therefore, it can be deduced that Al^{3+} and $(BO_3)^{3-}$ ions can be completely dissolved into the host lattice within the specified substitution range.

3.2. PL properties

It is well known that the distortion of the host lattice has a significant effect on the luminescence of Eu^{2+}, the luminescence property of NSAP:0.03Eu^{2+} and NSPB:0.03Eu^{2+} were recorded and displayed in Fig. 2. Fig. 2(a) and (b) show the excitation and emission spectra of NSA_xP:0.03Eu^{2+} ($0 \le x \le 1$), whilst, Fig. 2(d) and (e) exhibit the excitation and emission spectra of $NSPB_y$:0.03Eu^{2+} (y = 0.3, 0.5 and 1), respectively.

As shown in Fig. 2(a), with the increasing concentration of Al^{3+}, the tail of excitation spectrum is extended, which is more suitable for the commercial near-UV LED chip (360–420 nm). Meanwhile, as shown in Fig. 2(b), the emission of Eu^{2+} shows a slight shift to longer wavelength and is largely widened from a single symmetry band to asymmetry full-color band. The emission intensity is decreased and the emission width (FWHM) is increased as the substitution of Al^{3+} for Sc^{3+} in Fig. 2(c). Similarly, as exhibited in Fig. 2(d)-(f), the excitation and emission spectra are expanded while the emission intensity shows decrease with the increase of unit $(BO_3)^{3-}$. The broadening emission spectra are supposed to be caused by the mixing of several discrete emission centers. That is, Eu^{2+} can reside other different crystallographic sites caused by the equivalent cation or unit substitution.

To confirm the assumption, the deconvolution of the emission spectrum for the typical sample $NSA_{0.5}P$:0.03Eu^{2+} was carried. As shown in Fig. 3, the asymmetrical emission spectrum can be deconvoluted into three different bands centered at 17391.3 cm^{-1} (575 nm), 19880.7 cm^{-1} (503 nm) and 21881.8 cm^{-1} (457 nm). The emission band centered at 457 nm is identical to that of NSPO:0.03Eu^{2+}, which indicates that this emission originates from Eu^{2+} in eight-coordinated Na1 site [17].

According to the crystal structure of NSPO in Fig. 4(a), the compound NSPO, which belongs to monoclinic system structure, has three different Na sites Na1, Na2 and Na3. The Na1 ion is coordinated by eight O atoms with an average Na—O bond length of 2.6442 Å. Na2 is surrounded by seven O atoms with an average Na—O bond length of 2.60384 Å while Na3 is coordinated by six O atoms with an average Na—O bond length of 2.55606 Å. Either way, the three type polyhedrons of Na—O are corner shared with P—O tetrahedrons and Sc—O octahedrons. In general, the ligands can be distorted when the cation or unit is replaced by another one though with the same valence state. When doped into NSPO host, Eu^{2+} ions have priority to occupy the Na1 sites due to the closer ionic radii (r_{Na} = 1.18 Å, r_{Eu} = 1.25 Å, CN = 8) [19] and larger room of Na1—O polyhedron. As shown in Fig. 4(b) and (c), the original Sc—O octahedron or P—O tetrahedron is contracted when Sc or P is replaced by Al or B, due to the smaller ion radii of Al/B than that of Sc/P (r_{Al} = 0.535 Å, r_B = 0.11 Å, r_{Sc} = 0.74 Å, r_P = 0.44 Å, CN = 6) [19]. As a result, the average Na—O bond length is lengthened and the Na—O polyhedrons are stretched outward, which enables Na2 and Na3 to be replaced by Eu^{2+}. As known to all, for Eu^{2+} doped phosphor, the 5d energy level, which is responsive for the luminescence property, is strongly influenced by the local environment. Three main factors on the energetic level of 5d states are exhibited in Fig. 5. The centroid shift (ε_c) is related to nephelauxetic effect, which relies on the correlation between 5d and ligand electrons. The crystal field splitting (ε_{cfs}) of Eu^{2+} 5d states strongly depends on the ligand field strength neighboring the emission centers and the coordination geometry. The Stokes shift (ΔS), which determines the energetic difference between excitation and emission maximum, is governed by the vibration rigidity of the host lattice. According to Dorenbos, ε_c and ε_{cfs} can be expressed as followed equations (1) and (2), respectively [20].

$$\varepsilon_c = 1.79 \times 10^{13} \sum_{i=1}^{n} \frac{\alpha_{sp}^{i}}{(R_i - 0.6\Delta R)^6} \quad (1)$$

$$\varepsilon_{cfs} = \frac{\beta_{poly}}{R^2} \quad (2)$$

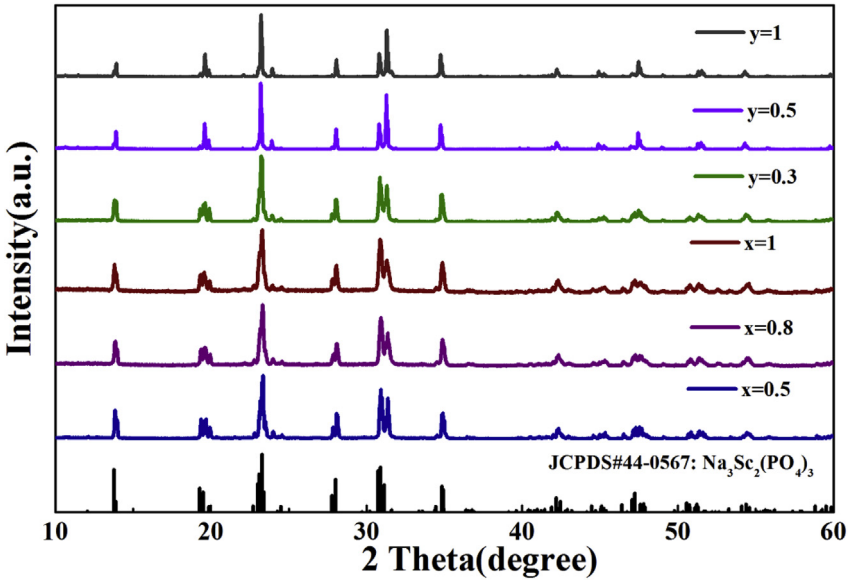

Fig. 1. XRD patterns for $NSA_xP:0.03Eu^{2+}$ (x = 0.5, 0.8 and 1) and $NSPB_y:0.03Eu^{2+}$ (y = 0.3, 0.5 and 1).

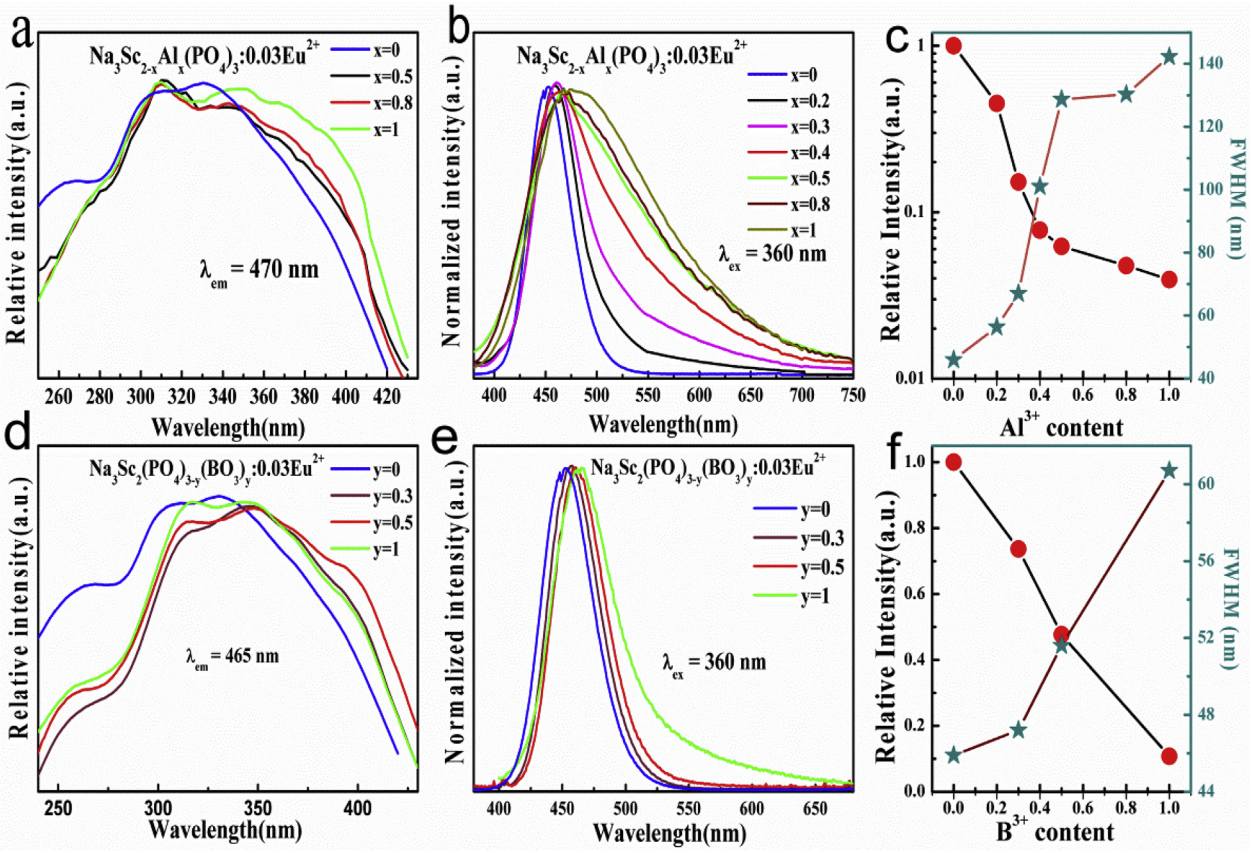

Fig. 2. The excitation and emission spectra of $NSA_xP:0.03Eu^{2+}$ ($0 \leq x \leq 1$) (a, b) and $NSPB_y:0.03Eu^{2+}$ ($0 \leq y \leq 1$) (d, e). The Al^{3+} and B^{3+} concentration dependence of the emission intensity and width (FWHM) (c and f).

As the cation Sc/P is replaced by a smaller one Al/B, the bond distance between Eu^{2+} and the surround coordinated anions will increase, which leads to the increase of ε_c and ε_{cfs}. Therefore, the energy difference between the 4f level and the lowest 5d level will be enlarged, which brings about the emission red shift of Eu1 as in Fig. 2(b) and (e). Additionally, for Eu^{2+} doped into a specific solid host material, ε_c and ΔS are most likely to be constant, which can be neglected in the excitation and emission shifts. The smaller polyhedron size generally indicates the shorter distance between Eu^{2+} and O^{2-} ligands, which result in the longer wavelength emission. Thereby, the longer emission bands 19880.7 cm^{-1} (503 nm) and 17391.3 cm^{-1} (575 nm) in Fig. 3 are attributed to Eu^{2+} in Na2 and Na3 sites, denoted as Eu2 and Eu3, respectively.

To further investigate the luminescence centers and the change of the emission spectra with the increase of Al^{3+} and B^{3+} content in $NSAP:0.03Eu^{2+}$ and $NSPB:0.03Eu^{2+}$. Under excitation at 360 nm, the

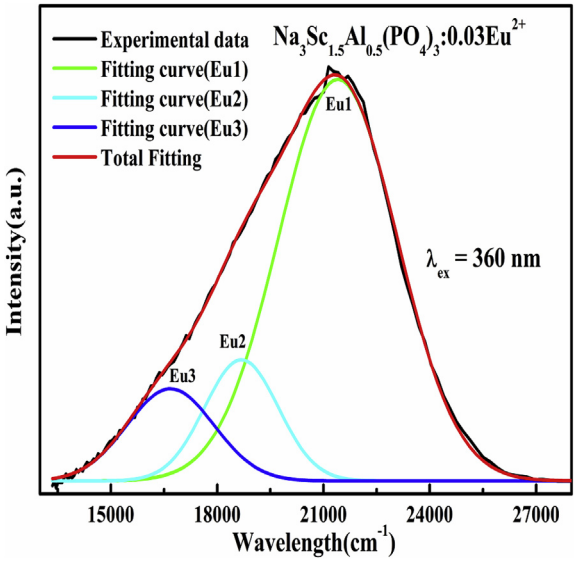

Fig. 3. Emission spectra of $Na_3Sc_{1.5}Al_{0.5}(PO_4)_3$:0.03$Eu^{2+}$ phosphors, λ_{ex} = 360 nm, experimental data (black solid line), fitted curve (red solid line) and deconvoluted Gaussian components (green, cyan and blue solid line). (For interpretation of the references to color in this figure legend, the reader is referred to the Web version of this article.)

samples of NSPO:0.03Eu^{2+}, NSAP:0.03Eu^{2+} and NSPB:0.03Eu^{2+} fluorescence lifetimes (τ) of Eu^{2+} were recorded and displayed in Fig. 6(a), (b) and (c), respectively. The decay curve (λ_{ex} = 360 nm, λ_{em} = 458 nm) of NSPO:0.03Eu^{2+} can be well fitted with single-exponential function and the lifetime of Eu^{2+} is 463.47 ns [18]. However, as shown in Fig. 6(b) and (c), the equivalent substitution of Sc by Al or $(PO_4)^{3-}$ by $(BO_3)^{3-}$ results in the deviation of Eu^{2+} fluorescence decay from single-exponential behavior. Instead, the decay curves of Eu^{2+} ions can be well fitted by the following bi-exponential function (3) [21,22].

$$I_{(t)} = A_1 e^{-t/\tau 1} + A_2 e^{-t/\tau 2} \quad (3)$$

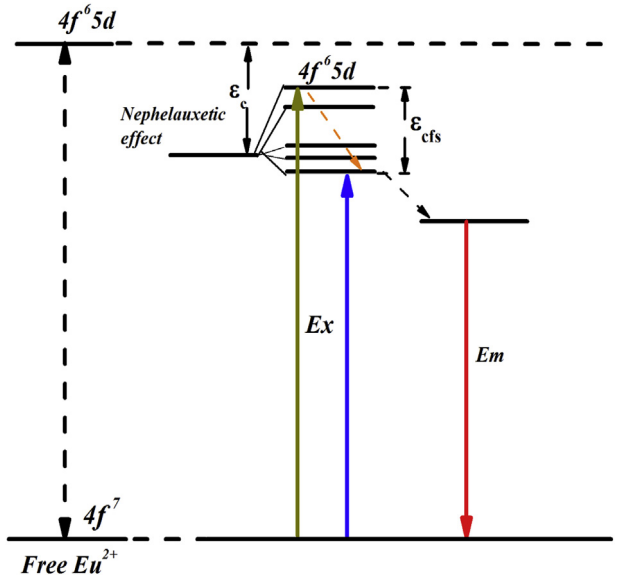

Fig. 5. The influence of the nephelauxetic effect and crystal field splitting on the 5d energy levels of Eu^{2+} ions.

Where $I_{(t)}$ is the luminescence Intensity, A_1 and A_2 are constants, t is the time, τ1 and τ2 are lifetimes for the exponential components. Further, the average decay time (τ) can be determined by the following formula [21]:

$$\tau = (A_1\tau_1^2 + A_2\tau_2^2)/(A_1\tau_1 + A_2\tau_2) \quad (4)$$

According to the above equation, the average lifetimes of Eu^{2+} in NSA_xP:0.03Eu^{2+} (x = 0.5, 0.8 and 1) are calculated to be 286.23, 259.8 and 201.88 ns (λ_{ex} = 360 nm, λ_{em} = 470 nm). The effective lifetime values of Eu^{2+} in the samples of $NSPB_y$:0.03Eu^{2+} (y = 0.3, 0.5 and 1) are also calculated, to be 479.8, 444.12 and 378.12 ns respectively. These resulting indicate that the influence of Al^{3+} replace Sc^{3+} is more obvious than $(BO_3)^{3-}$ replace $(PO_4)^{3-}$ in the NSPO host, which is consistent with the spectral results (in Fig. 3). Since the lifetimes of Eu^{2+} at

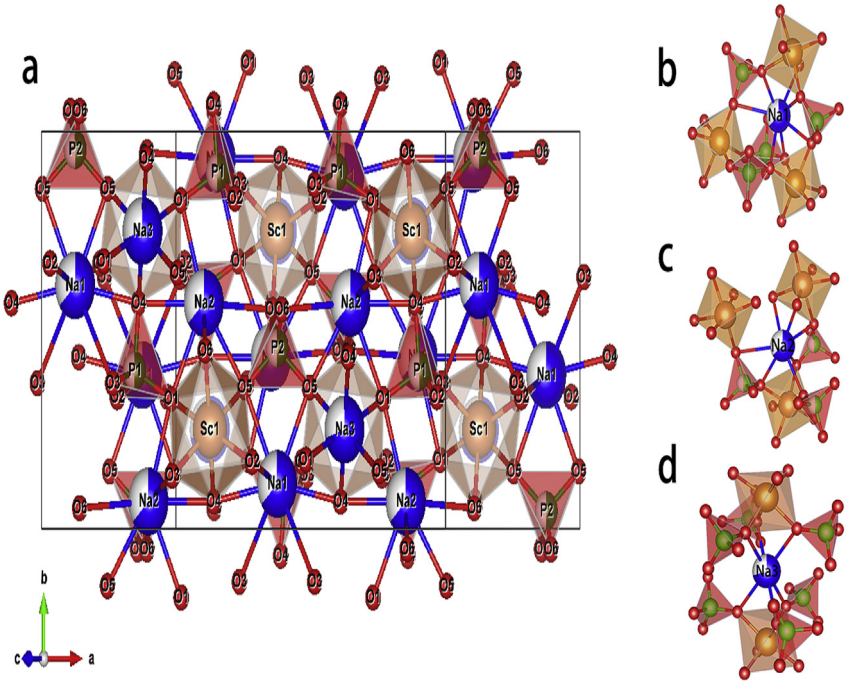

Fig. 4. Crystal structure of $Na_3Sc_2(PO_4)_3$ cell viewed in c-direction (a) and the coordination environment of Na1 (b), Na2 (c) and Na3 (d) in $Na_3Sc_2(PO_4)_3$.

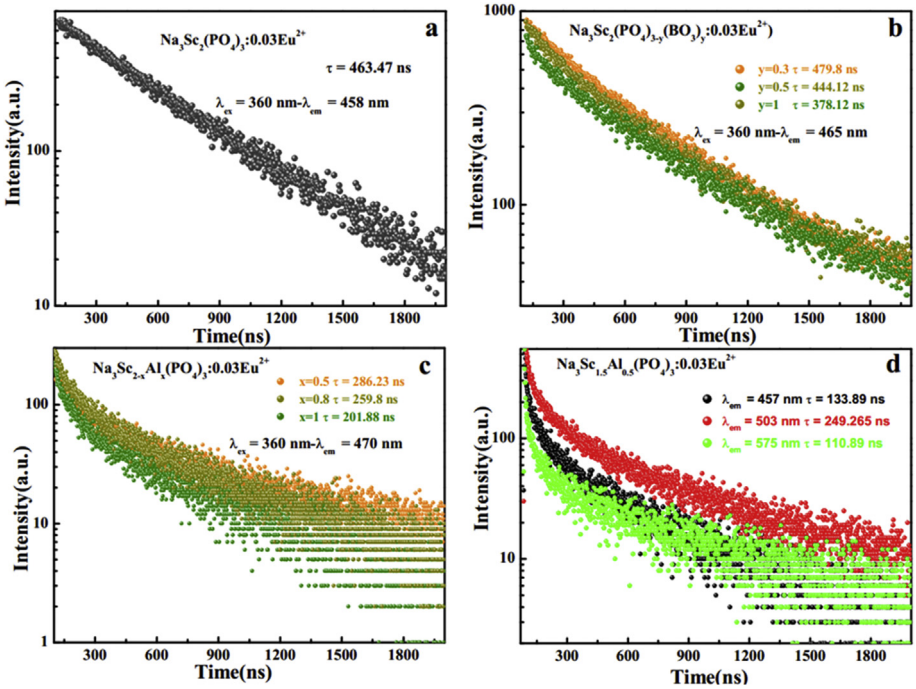

Fig. 6. The lifetime decay curves of NSA_xP:0.03Eu^{2+} ($0 \le x \le 1$) and $NSPB_y$:0.03Eu^{2+} ($0 \le y \le 1$) (a, b and c), the lifetime decay curves of three emission bands λ_{em} = 457, 503 and 575 nm of $NSA_{0.5}P$:0.03Eu^{2+} (d).

different sites are different, thus it is an efficient method of measuring the decay lifetimes to identify the sites of Eu^{2+} ions [11]. Hence, the decay curves of NSAP:0.03Eu^{2+} monitored at three different emissions (λ_{em} = 457, 503 and 575 nm) are displayed in Fig. 6(d). The average lifetimes of Eu^{2+} at different emission (457, 503 and 575 nm) are calculated to be 133.89, 249.265 and 110.89 ns, which proves the occupation of Eu^{2+} ions in three different sites.

3.3. Thermal stability

Thermal stability is one of the most important characters for a phosphor utilized in w-LEDs. Fig. 7 shows the temperature dependence of emission spectra and the integral emission intensity for $NSA_{0.5}P$:0.03Eu^{2+} and $NSPB_{0.3}$:0.03Eu^{2+} phosphors at evaluated temperature from 303 to 523 K under 360 nm excitation are given. With the temperature ascends, the $NSA_{0.5}P$:0.03Eu^{2+} phosphors emission intensity show an significant decrease, as shown in Fig. 7(a). Meanwhile, the integral emission intensity (black dotted line)) also is shown in Fig. 7(c) which indicates that the substitution of Al for Sc has a great effect on the thermal quenching behavior. Furthermore, in Fig. 7(a), it also can be found that the thermal stability of Eu1 is better than that of Eu2 and Eu3 emission, which further verified the three different emission centers.

As shown in Fig. 7(b) and (d), compared with the initial intensity at room temperature, $NSPB_{0.3}$:0.03Eu^{2+} phosphor shows anti-thermal quenching behavior and reaches a maximum at T = 373 K. However, sample NSAP:0.03Eu^{2+} shows serious thermal quenching behavior. In order to explain the different thermal quenching behaviors, the thermoluminescence curves of NSPO:0.03Eu^{2+}, $NSA_{0.5}P$:0.03Eu^{2+} and $NSPB_{0.3}$:0.03Eu^{2+} were given in Fig. S1. The thermoluminescence curve of NSPO:0.03Eu^{2+} shows two prominent trap levels at 40–135 °C and 135–250 °C, which greatly contributes to the good thermal stability. In contrast, the two traps of sample $NSPB_{0.3}$:0.03Eu^{2+} shift to lower temperature side, which results in thermal quenching at much lower temperature (373 K). Moreover, the extremely weak thermoluminescence curve of sample $NSA_{0.5}P$:0.03Eu^{2+} indicates low trap density and leads to the terrible thermal stability [23].

The temperature-dependent decay lifetime curves are one of the most important methods to investigate thermal quenching response at different emission centers [24]. The decay curves of the three emissions (λ_{em} = 457, 503 and 575 nm) at different temperature were recorded (λ_{ex} = 360 nm), as shown Fig. 8(a), (b) and (c). The fluorescence lifetimes of Eu^{2+} (457, 503 and 575 nm) at 483 K can be calculated to be 107.84, 127.98 and 60.12 ns. Compared with the lifetimes at room temperature, the fluorescence lifetime change of emission center at 503 and 575 nm is more obvious than that of 457 nm. The phenomenon can be ascribed to Eu^{2+} occupy different Na^+ sites and demonstrates that Eu1 emission is more thermally stable.

The emission color can be manifested in a CIE chromaticity diagram. The chromaticity coordinates of NSA_xP:0.03Eu^{2+} and $NSPB_y$:0.03Eu^{2+} are shown in Fig. 9 and Table 1. Evidently, the emission color of NSA_xP:0.03Eu^{2+} ($0 \le x \le 1$) can be adjusted from deep blue (0.1431, 0.0643) to green (0.2536, 0.3279) with the increasing of Al^{3+} content. Meanwhile, the emission color of $NSPB_y$:0.03Eu^{2+} ($0 \le y \le 1$) can be adjusted from deep blue (0.1431, 0.0643) to light blue (0.2266, 0.2155) as the increase of B^{3+} content.

4. Conclusions

In summary, NSAP:0.03Eu^{2+} and NSPB:0.03Eu^{2+} phosphors were prepared by high temperature solid state method. With the increasing of Al^{3+} and $(BO_3)^{3-}$ content, the emission spectrum of Eu^{2+} in NSPO is widened, which is attributed to the controlling the multi-emission centers that the creation of new occupation sites (Na2 and Na3) for Eu^{2+} as the stretched Na2—O and Na3—O polyhedrons. Meanwhile, the thermal stability was investigated and the mechanism of widening the Eu^{2+} emission spectrum was also elucidated.

Declaration of interests

None.

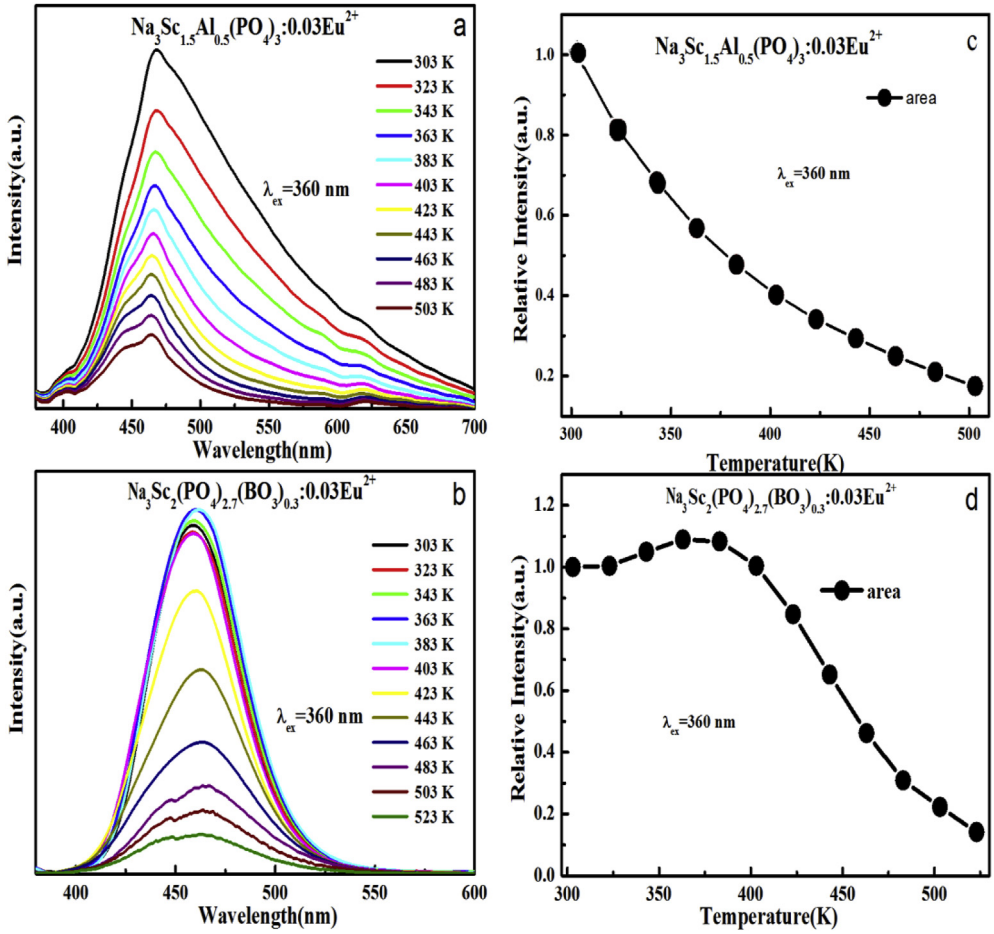

Fig. 7. Temperature-dependent emission spectra and integrated luminescence intensity of $NSA_{0.5}P:0.03Eu^{2+}$ and $NSPB_{0.3}:0.03Eu^{2+}$.

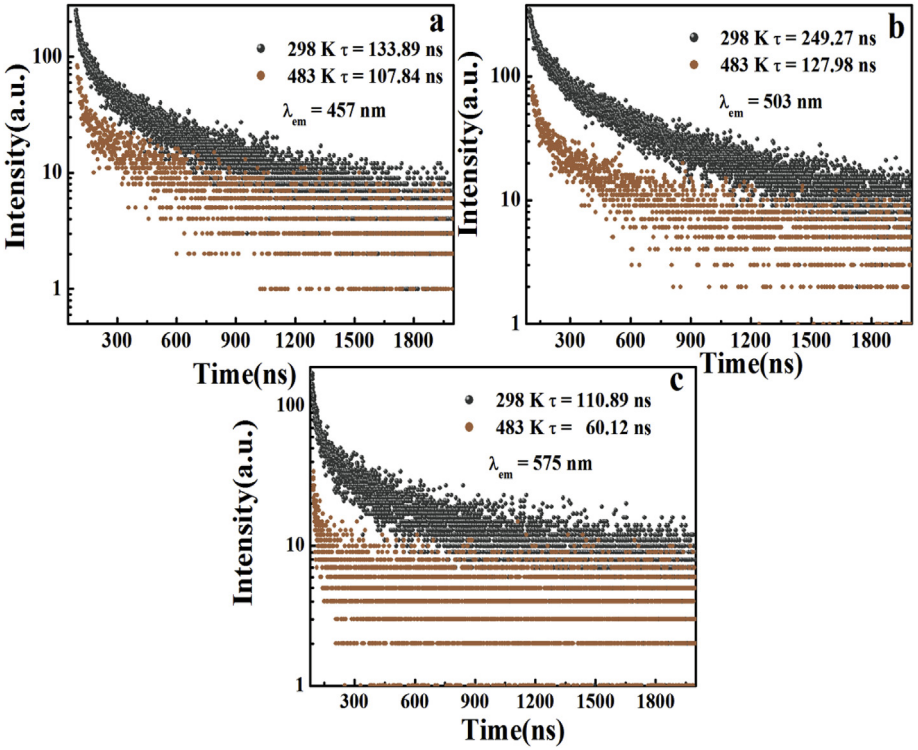

Fig. 8. The temperature-dependent lifetimes (τ) of different emission (λ_{em} = 457 nm) (a), (λ_{em} = 503 nm) (b) and (λ_{em} = 575 nm) (c) of $NSA_{0.5}P:0.03Eu^{2+}$.

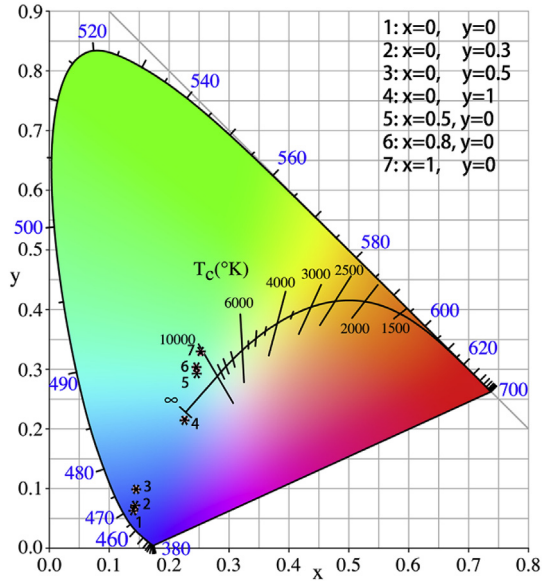

Fig. 9. CIE chromaticity coordinates of NSA_xP: $0.03Eu^{2+}$ and $NSPB_y$:$0.03Eu^{2+}$ phosphors.

Table 1
CIE chromaticity coordinates for samples $Na_3Sc_{2-x}Al_x(PO_4)_{3-y}(BO_3)_y$:$0.03Eu^{2+}$ under excitation at 360 nm.

No.	$Na_3Sc_{2-x}Al_x(PO_4)_{3-y}(BO_3)_y$:$0.03Eu^{2+}$		CIE(x)	CIE(y)
1	x = 0	y = 0	0.1431	0.0643
2	x = 0	y = 0.3	0.1432	0.0691
3	x = 0	y = 0.5	0.1455	0.0983
4	x = 0	y = 1	0.2266	0.2155
5	x = 0.5	y = 0	0.2462	0.2987
6	x = 0.8	y = 0	0.2452	0.3022
7	x = 1	y = 0	0.2536	0.3279

Acknowledgements

The authors acknowledge the financial support from the National Natural Science Foundation of China (No. 21676045); National Natural Science Foundation of China (No. 51802045); Special Fund for Scientific and Technological Innovation Strategy of Guangdong Province (No.2018A030310539); and Youth Innovation Talent Project of Education Department of Guangdong Province, China (No. 2016KQNCX041).

Appendix A. Supplementary data

Supplementary data to this article can be found online at https://doi.org/10.1016/j.optmat.2018.12.038.

References

[1] P. Pust, P.J. Schmidt, W. Schnick, A revolution in lighting, Nat. Mater. 14 (2015) 454–458.
[2] J.S. Kim, P.E. Jeon, J.C. Choi, H.L. Park, S.I. Mho, G.C. Kim, Warm-white-Light emitting diode utilizing a single-phase full-color $Ba_3MgSi_2O_8$:Eu^{2+}, Mn^{2+} phosphor, Appl. Phys. Lett. 84 (2004) 2931–2933.
[3] M. Krings, G. Montana, R. Dronskowski, C. Wickleder, α-SrNCN:Eu^{2+} – a novel efficient orange-emitting phosphor, Chem. Mater. 23 (2011) 1694–1699.
[4] X. Li, J.D. Budai, F. Liu, J.Y. Howe, J. Zhang, X. Wang, Z. Gu, C. Sun, R.S. Meltzer, Z. Pan, New yellow $Ba_{0.93}Eu_{0.07}Al_2O_4$ phosphor for warm-white light-emitting diodes through single-emitting-center conversion, Light Sci. Appl. 2 (2013) e50.
[5] A.A. Setlur, W.J. Heward, M.E. Hannah, U. Happek, Incorporation of Si^{4+}–N^{3-} into Ce^{3+}-doped garnets for warm white LED phosphors, Chem. Mater. 20 (2008) 6277–6283.
[6] C.K. Chang, T.M. Chen, $Sr_3B_2O_6$:Ce^{3+}, Eu^{2+}:A potential single-phased white-emitting borate phosphor for ultraviolet light-emitting diodes, Appl. Phys. Lett. 91 (2007) 46.
[7] X. Zhang, X. Qiao, H.J. Seo, Luminescence properties of novel Ce^{3+}, Mn^{2+} doped $NaSr_4$ $(BO_3)_3$ phosphors, Curr. Appl. Phys. 11 (2011) 442–446.
[8] Y. Zhang, G. Li, D. Geng, M. Shang, C. Peng, J. Lin, Color-tunable emission and energy transfer in $Ca_3Gd_7(PO_4)(SiO_4)_5O_2$:$Ce^{3+}$/$Tb^{3+}$/$Mn^{2+}$ phosphors, Inorg. Chem. 51 (2012) 11655–11664.
[9] W. Lü, Z. Hao, X. Zhang, Y. Luo, X. Wang, J. Zhang, Tunable full-color emitting $BaMg_2Al_6Si_9O_{30}$: Eu^{2+}, Tb^{3+}, Mn^{2+} phosphors based on energy transfer, Inorg. Chem. 50 (2011) 7846–7851.
[10] M. Tian, P. Li, Z. Wang, Z. Li, J. Cheng, Y. Sun, C. Wang, X. Teng, Z. Yang, F. Teng, Controlling multi luminescent centers via anionic polyhedron substitution to achieve single Eu^{2+} activated high-color-rendering white light/tunable emissions in single-phased $Ca_2(BO_3)_{1-x}(PO_4)_xCl$ phosphors for ultraviolet converted LEDs, Chem. Eng. J. 326 (2017) 667–679.
[11] Q. Zhang, Q. Wang, X. Wang, X. Ding, Y. Wang, Luminescence properties of Eu^{2+}-doped $BaSi_2O_5$ as an efficient green phosphor for light-emitting devices and wide color gamut field emission displays, New J. Chem. 40 (2016) 8549–8555.
[12] P. Dorenbos, Energy of the first $4f^7 \rightarrow 4f^6 5d$ transition of Eu^{2+} in inorganic compounds, J. Lumin. 104 (2003) 239–260.
[13] W.R. Liu, C.H. Huang, C.W. Yeh, Y.C. Chiu, Y.T. Yeh, R.S. Liu, Single-phased white-light-emitting $KCaGd(PO_4)_2$:Eu^{2+}, Tb^{3+}, Mn^{2+} phosphors for LED applications, RSC Adv. 3 (2013) 9023–9028.
[14] Y.J. Chen, L. Chen, L.J. Xiao, Y. Yang, X.J. Geng, Y. Xie, S.N. Wu, The effect of different lattice sites substitution on photoluminescence characteristics of Eu^{2+}/Ce^{3+} doped $M_5(ZO_4)_3X$, Mater. Sci. Semicond. Process. 18 (2014) 59–64.
[15] H. Yu, D. Deng, Y. Hua, C. Li, S. Xu, Orange- to green- emitting $Li(Sr,Ca)_4(BO_3)_3$:Eu^{2+} phosphor: emission-tunable properties and white light emitting diodes application, RSC Adv. 6 (2016) 82824–82831.
[16] X. Wang, Z. Zhao, Q. Wu, C. Wang, Q. Wang, Y. Li, Y. Wang, Structure, photoluminescence and abnormal thermal quenching behavior of Eu^{2+}-doped $Na_3Sc_2(PO_4)_3$:a novel blue-emitting phosphor for n-UV LEDs, J. Mater. Chem. C 4 (2016) 8795–8801.
[17] Y.H. Kim, P. Arunkumar, B.Y. Kim, S. Unithrattil, E. Kim, S.H. Moon, J. Hyun, K. Kim, D. Lee, J.S. Lee, W.B. Im, A zero-thermal-quenching phosphor, Nat. Mater. 16 (2017) 543–550.
[18] D. Liu, Y. Jin, Y. Lv, G. Ju, C. Wang, W. Luo, C. Li, Y. Hu, A single-phase full-color emitting phosphor $Na_3Sc_2(PO_4)_3$:Eu^{2+}/Tb^{3+}/Mn^{2+} with near zero-thermal quenching and high quantum yield for near-UV converted warm w-LEDs, J. Am. Ceram. Soc. 101 (2018) 5627–5639.
[19] R.D. Shannon, Revised effective ionic radii and systematic studies of interatomic distances in halides and chalcogenides, Energy Harvesting & Systems 32 (1976) 751–767.
[20] P. Dorenbos, 5d-level energies of Ce^{3+} and the crystalline environment. III. Oxides containing ionic complexes, Phys. Rev. B 64 (2001) 125117.
[21] X. Liu, L. Yan, J. Lin, Synthesis and luminescent properties of $LaAlO_3$:RE^{3+} (RE = Tm, Tb) nanocrystalline phosphors via a sol—gel process, J. Phys. Chem. C 113 (2009) 8478–8483.
[22] Y. Liu, J. Hao, W. Zhuang, Y. Hu, Structural and luminescent properties of gel-combustion synthesized green-emitting $Ca_3Sc_2Si_3O_{12}$:Ce^{3+} phosphor for solid-state lighting, J. Phys. D Appl. Phys. 42 (2009) 245102 (6pp).
[23] L. Jin, H. Zhang, R. Pan, P. Xu, J. Han, X. Zhang, Y. Wang, B. Song, Observation of the long afterglow in AlN helices, Nano Lett. 15 (2015) 6575–6581.
[24] D. Chen, X. Chen, X. Li, H. Guo, S. Liu, X. Li, Cr^{3+}-doped $Bi_2Ga_4O_9$-$Bi_2Al_4O_9$ solid-solution phosphors: crystal-field modulation and lifetime-based temperature sensing, Opt. Lett. 42 (2017) 4950–4953.